# Equivalence ratio measurements in kerosene-fuelled LPP injectors using planar laser-induced fluorescence

**Mikaël Orain[1], Hubert Verdier[2], Frédéric Grisch[3]**

1: Physics, Instrumentation and Sensing Department, Office National d'Etudes et de Recherches Aérospatiales, Palaiseau, France, mikael.orain@onera.fr
2: Combustion Chambers Department, Turboméca, Bordes, France, Hubert.verdier@turbomeca.fr
3: Physics, Instrumentation and Sensing Department, Office National d'Etudes et de Recherches Aérospatiales, Palaiseau, France, frederic.grisch@onera.fr

**Abstract** The quantitative PLIF-kerosene technique developed by Baranger et al. (2005) was applied for the first time to a real LPP injector operating at atmospheric pressure with jet A1 fuel, for air temperature between 500 and 650 K and overall equivalence ratio in the range 0.12–0.44. Instantaneous images of kerosene fluorescence were recorded for evaporating conditions (i.e. no combustion, only fuel vaporisation) with two ICCD cameras equipped with appropriate optical filters. Fluorescence images were processed using the dependencies found by Baranger et al. (2005) in order to obtain maps of local equivalence ratio. Influence of air temperature and air and fuel flowrates on local equivalence ratio was investigated. Results indicate fuel vaporisation rates between 35 and 55 %, depending on temperature and fuel loading. A region of fairly homogeneous equivalence ratio extending axially over about half the diameter of the premixing duct is clearly visible at the exit of the LPP system. It was also observed that kerosene fuel does not spread over all the section of the premixing duct.

## 1. Introduction

Increasingly stringent regulations on pollutant emissions, such as $NO_x$, $CO_x$ and soot, require to improve combustion efficiency and overall operability of kerosene-fuelled aeronautical gas turbines. Among key parameters likely to fulfil these goals, the injection system is one of them where substantial improvements can still be achieved. For example, it is well known that atomisation of liquid jets (shear-coaxial injectors) occurs via different physical processes compared to break-up of liquid sheets (film injectors), which often results in different droplet size, velocity and density (Pilch and Erdman, 1987; Lefebvre, 1989). Therefore, optimisation of the atomisation of liquid fuel into fine droplets and their subsequent evaporation is of great importance for fuel spatial distribution within the combustor (Lefebvre, 1999; Turns, 2000; Lefebvre, 1995). Additionally, efficient mixing between preheated combustion air and fuel vapour generated by droplet evaporation is crucial to combustion efficiency. First, in terms of pollutant emissions, which can be greatly reduced if the spatial distribution of air/fuel mixture in the combustor is homogeneous with lean equivalence ratio (Cheng et al., 2001; Fric, 1993; Terasaki and Hayashi, 1996). This yields lower flame temperature (1500-1800 K), hence lower $NO_x$ emissions, and the absence of fuel-rich pockets leads to reduced soot formation. Second, in terms of combustion instabilities, which are known to partly depend on temporal and spatial inhomogeneities of the air/fuel mixture in the combustion chamber (Lieuwen and Zinn, 1998; Cohen et al., 2001; Sattelmayer, 2003). Such instabilities are naturally not compatible with standards of reliability, durability and drivability required for aircrafts engines, and, therefore, must be avoided.

Over the last two decades, intensive research has been dedicated to improve existing injection systems and to imagine innovative designs. This has led to new concepts like LP (Lean Premixed) and LPP (Lean Premixed Prevaporised) injectors which contribute to match the targeted goals of future regulations on pollutants emissions, Correa (1992). The principle of these injectors is to

atomise the liquid fuel into small droplets which evaporate to a large extent, and mix the subsequent fuel vapour with air in a prevaporising/premixing duct, in order to obtain a fairly homogeneous air/fuel mixture before combustion occurs. Many experiments have used laser-based techniques to determine the influence of parameters like droplet size and velocity, air temperature, fuel and air flowrates on the performances of such injectors (Löfström et al., 2000; Greenhalgh, 2000; Martins et al., 2004). However, these studies were mainly focused on the spatial distribution of liquid phase in the combustor, and the evolution of droplet size at different locations from the injector exit was used to estimate fuel evaporation (Michou et al., 1999; Becker and Hassa, 2003; Subramaniyam, 2004). Indeed, only few experiments were performed to characterise fuel vapour phase (Stufflebeam et al., 2002; Galley et al., 2004; Krämer et al., 1999). In addition, results were typically obtained with surrogate fuels or added tracers which were not necessarily representative of typical fuels used in aircraft engines (i.e. kerosene). Therefore, it may be that the conclusions drawn from these experiments were biased by the type of fuel they used, because of the different evaporation behaviour and combustion processes of surrogates or tracers compared to that of real fuels. Only very few examples of studies performed with optical diagnostics directly applied to kerosene vapour are available in the literature (Hicks et al., 1997; Locke et al., 1999; Arnold et al., 2000; Nguyen et al., 1999). Unfortunately, these results were only qualitative, because kerosene spectroscopy was not properly established despite the pioneering work of Löfström et al. (1996). Recently, Baranger et al. (2005) have thoroughly investigated kerosene spectroscopy for various conditions of temperature, pressure and oxygen molar fraction. These authors have identified molecular species responsible for kerosene fluorescence and they have derived a strategy for measuring local equivalence ratio in kerosene-fuelled gas turbines using Planar Laser-Induced Fluorescence (PLIF). Potential of the technique was preliminarily demonstrated on a gaseous jet of kerosene/$N_2$ heated at 650 K, and then its applicability to two-phase flows was established on a kerosene-fuelled nozzle from a domestic boiler.

The goal of the present experiments was to apply PLIF-kerosene to an LPP injector operating with kerosene (jet A1) at atmospheric pressure for non-reactive conditions (i.e. no combustion, only fuel vaporisation). Influence of air temperature at the inlet (between 500 and 650 K) and overall equivalence ratio (in the range 0.12–0.44) on the spatial distribution of local equivalence ratio within the combustor was investigated. The remaining paper comprises three sections. The next section describes the experimental set-up. The second section presents and discusses the results. Finally, the paper ends with a summary of the main findings.

## 2. Experimental set-up

### Combustor

The test rig, represented in Fig. 1, comprised a 6.2 kW electrical heater which can preheat air up to 900 K for a 10 g/s air flowrate. The heater was connected to the combustor which comprised three parts made of stainless steel. The first part was a cylinder which contains glass beads in order to homogenise the airflow. The fuel supply line was located on the cylinder axis and it was encapsulated in a water-cooled jacket to ensure that the temperature of liquid kerosene remained constant during experiments. The water jacket itself was also covered with ceramics to minimise heat losses. The LPP system, designed by Turboméca (TM), was fixed at the top of the fuel supply line. The second part of the combustor corresponded to the water-cooled visualisation sector. It was equipped with three optical access made with UV-silica windows, one of which was used for laser access and the two others for detecting kerosene fluorescence with ICCD cameras. It is necessary to mention that the visualisation sector was equipped with an anti-recirculation plate connected to the LPP system, which ensured that no fuel vapour or air could recirculate upstream from the

prevaporising duct. In addition, optical access was specifically designed so that kerosene fluorescence could be collected right at the exit of the LPP system. Finally, the third part of the combustor was a water-cooled cylinder connected to the extraction system. Air was supplied by the laboratory compressor and its flowrate was controlled by a mass flowmeter in the range 0–10 g/s with 0.2 % uncertainty. Liquid kerosene was stored in a pressurised tank and its flowrate was controlled by a mass flowmeter in the range 0–13 kg/h with 0.2 % accuracy. Air flowrate was kept constant and overall equivalence ratio ($\Phi_0$) was varied between 0.12 and 0.44. Air temperature at the exit of the LPP system varied between 500 and 650 K, and it was controlled with a type-K thermocouple which was used to input the PID regulation system of the heater.

The origin of the co-ordinate system used in the following is located on the combustor axis at the exit of the LPP system. The term "axial direction" (z axis) refers to the combustor axis, while the term "radial direction" (r axis) stands for the direction perpendicular to the flow axis. The diameter of the premixing duct ($D_0$) is used as a scaling parameter for spatial co-ordinates, so that profiles of equivalence ratio are displayed as a function of $r/D_0$ or $z/D_0$.

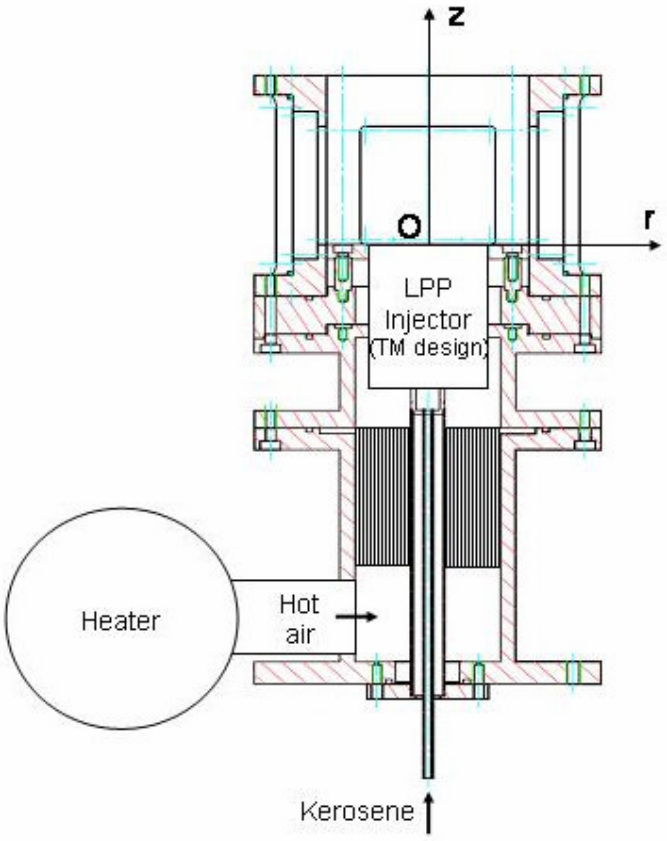


Figure 1. Experimental test rig.

## Optical set-up

The optical set-up used for the current experiments was similar to that used by Baranger et al. (2005) and is schematically represented in Fig. 2. It was a single-excitation scheme which comprises a frequency-quadrupled Nd:YAG laser generating 8 ns, 50 mJ pulses at 266 nm. The laser beam was transformed into a collimated sheet using a combination of cylindrical and spherical lenses. The two cylindrical lenses, -20 mm and 300 mm focal lengths, formed a cylindrical telescope which spread the beam into a collimated, 50 mm high sheet. The spherical lens, 900 mm

focal length, focused the sheet to a 130 μm waist. The laser sheet impacted the mixture jet and fluorescence from kerosene vapour and liquid phases was simultaneously recorded with two facing 16-bit ICCD cameras with a temporal gate of 200 ns. The CCD array was 512×512 pixels and the framing rate of the system was fixed at 3 Hz. Both ICCD cameras were equipped with a *f*/4.1, *f*=94 mm, achromatic UV lens. The first camera was equipped with a WG 280 Schott filter to collect the whole fluorescence of kerosene, whereas the second camera used a WG 305 Schott filter to collect fluorescence from di-aromatics only. Each camera was interfaced to a personal computer used to control the camera and to record the images.

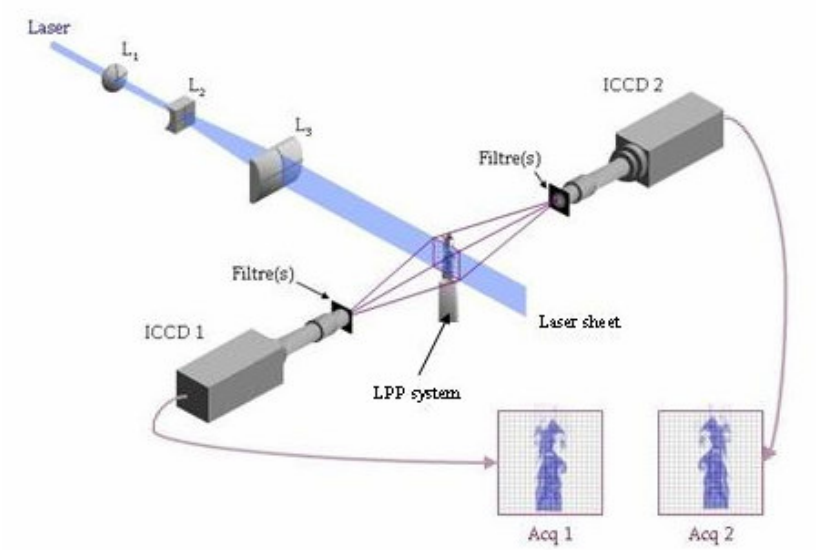


Figure 2. Schematic of the optical set-up.

## 3. Results

This section presents PLIF measurements of local equivalence ratio at the exit of the LPP injector for non-reactive conditions. The first part of the section concerns the data processing used for converting fluorescence raw images into maps of local equivalence ratio. The second part presents the results for three flow conditions. Influence of overall equivalence ratio ($\Phi_0$) on the spatial distribution of local equivalence ratio in the combustor is first examined and then effect of inlet temperature is determined for a given $\Phi_0$.

### Data processing

Figure 3 presents a typical instantaneous raw image of kerosene fluorescence after illumination of the flow by the laser sheet from top to bottom. The bright dots, representing large intensities, correspond to droplets, while fuel vapour is displayed with a false colorscale. The gain of both ICCD cameras was adjusted to keep the energy recorded by the array detector proportional to the fluorescence signal issued from the liquid and gas phases, which prevents the ICCD cameras from local saturation and blooming induced by the liquid kerosene fluorescence. For each flow condition, 200 single-shot images were acquired with each ICCD camera and the maps of mean local equivalence ratio presented in this article result from the average over these 200 single-shots.

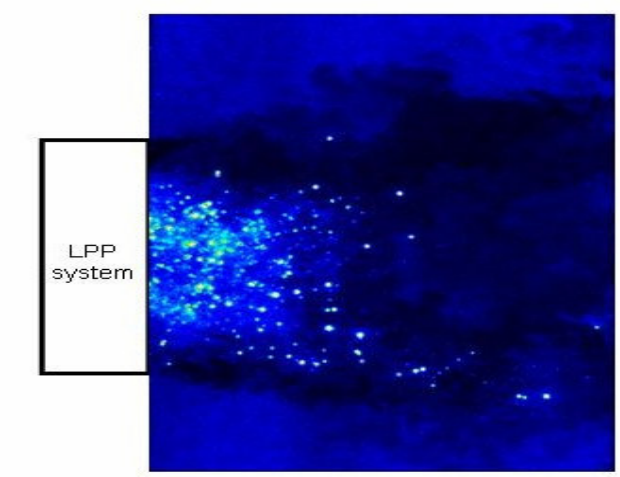


Figure 3. Fluorescence intensity emitted by kerosene vapour and droplets in the combustor (T=500 K, $\Phi_0$=0.12).

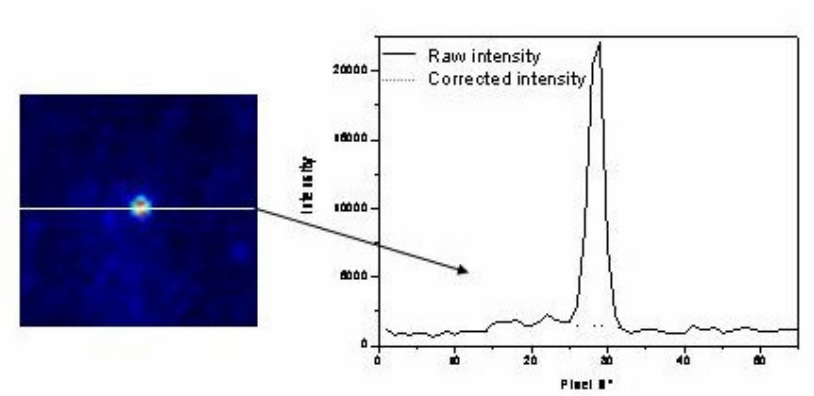


Figure 4. Procedure used to interpolate fluorescence intensity over a droplet area.

Before obtaining quantitative information from fluorescence images, the recorded images had to be processed and corrected to ensure validity and reliability of the measurements. Errors influencing the measurements quality mainly derived from camera system noise, laser scattering, reflections, non-uniformity of the laser sheet and fluctuations of the laser power. Halation phenomenon was not found to be an important source of uncertainty here, as opposed to our observations in a previous article (Orain et al., 2005), because the magnification adopted for the current experiments is much lower (1:0.44 *vs.* 1:2.6). Data reduction of fluorescence images is now detailed. First, an average background image was acquired with the laser on, but without any kerosene injected in the combustor. Subtraction of this image from the fluorescence image accounted for laser scattering and other background luminosity. Second, in order to remove the effects of non-uniformities in the collection optics as well as variations in the laser sheet profile, an image was acquired of a room-temperature airflow seeded with constant acetone vapour concentration. With the assumption, supported by examination of the images, that the laser sheet profile and energy remained constant, division by this suitably background-subtracted image corrected for optical non-uniformities and laser sheet variations. Finally, data processing used to convert fluorescence images into maps of local equivalence ratio was the same as that developed by Baranger et al. (2005). It consisted of using the dependencies upon temperature and oxygen molar fraction of kerosene fluorescence obtained from previous spectroscopic measurements. These dependencies were incorporated in an iterative procedure which compares, for each pixel, the fluorescence intensity collected by each ICCD camera. Fluorescence intensity was then converted into local equivalence ratio. However, with the present experiments, it was necessary to add an extra routine which takes account of the presence of kerosene droplets in the flow. Due to the

difference of density between the liquid and vapour phases of kerosene, fluorescence signals were significantly larger for the liquid phase. As a result, there was a strong intensity gradient between a droplet and its surrounding vapour. We took advantage of this feature to identify the location of droplets and to eliminate the fluorescence signal from the liquid phase which was initially set to zero. The fluorescence signal at the droplet location was then interpolated over the droplet area using the value of fluorescence intensity from kerosene vapour at the first pixel around the droplet both in the radial and axial directions. This procedure is detailed in Fig. 4 along one direction only.

**Condition 1 (T=500 K, $\Phi_0$=0.12)**

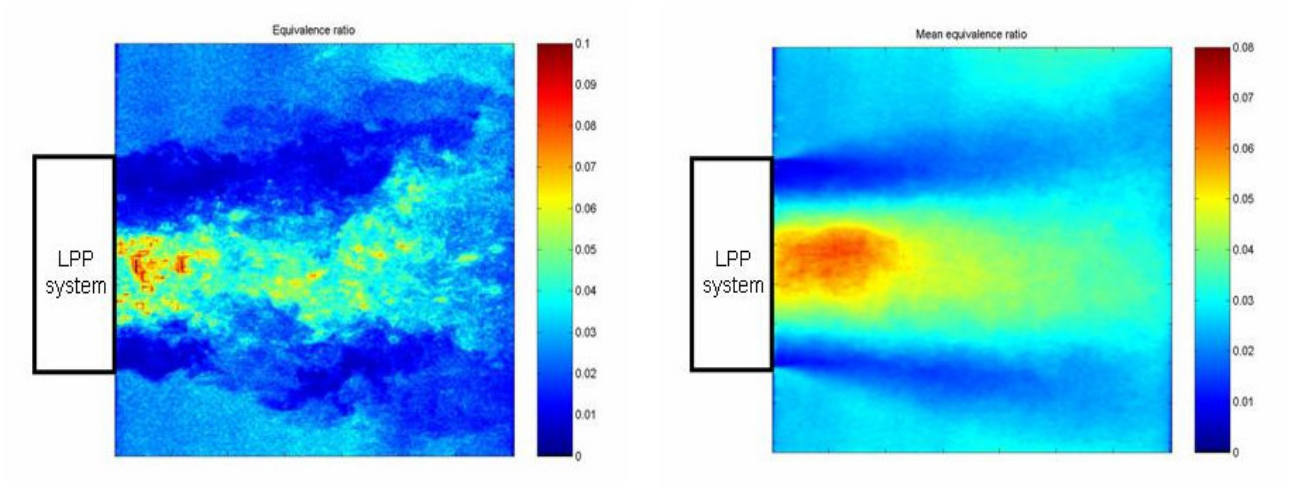


(a) (b)

Figure 5. Instantaneous (a) and average over 200 images (b) maps of local equivalence ratio for condition 1 (T=500 K, $\Phi_0$=0.12).

For this first case, fluorescence images were recorded with an inlet temperature of T=500 K and an overall equivalence ratio of $\Phi_0$=0.12. Figure 5-a shows an instantaneous map of local equivalence ratio ($\Phi$) obtained with the procedure described above. As can be seen, the kerosene/air jet is fairly directional and exhibits little radial expansion with axial distance. In addition, kerosene vapour remains mainly located along the combustor centreline, and, in particular, its radial extent at the exit of the LPP system does not exceed half the diameter of the premixing duct ($D_0$). Indeed, almost no fuel vapour (or liquid kerosene) can be detected close to the edge of the duct (i.e. $-0.5<r/D_0<-0.2$ and $0.2<r/D_0<0.5$). It is remarkable that this confinement persists over an axial distance of the order of $D_0$, which can be more conveniently seen in Fig. 5-b. This may be due to swirl effects which create a "shield" that prevents kerosene vapour to reach that radial location. Or alternatively, as the overall equivalence ratio is very low ($\Phi_0$=0.12), little fuel is available to spread radially. On each side of the premixing duct, occurrence of kerosene vapour is noted. This results from the recirculation zones present at that location which transport and trap fuel vapour at the edges of the combustor. The average map of local equivalence ratio in Fig. 5-b shows that $\Phi$ is fairly homogeneously distributed over a region with $-0.17<r/D_0<0.17$ and $0<z/D_0<0.45$. In that zone, local equivalence ratio remains between 0.06 and 0.07; while further downstream, $\Phi$ lies in the range 0.03–0.05. This demonstrates that the ratio $\Phi/\Phi_0$, which is representative of the kerosene vaporisation rate, is about 55 % at the exit of the LPP system. This suggests fairly good evaporation of kerosene fuel. This comes from two combined effects: first, inlet temperature, although limited to 500 K, enhances fuel vaporisation; second, the overall equivalence ratio is very low ($\Phi_0$=0.12) and, therefore, only little kerosene is to evaporate. The decrease of local equivalence ratio observed for $z/D_0>0.7$ is mainly due to dilution with air, initially located at the periphery of the kerosene/air jet, that enters the jet and mixes with kerosene vapour. Radial expansion of the jet is limited and,

therefore, it is only marginally responsible for this reduction of local equivalence ratio. As mentioned previously, regions with $\Phi$~0.01 are clearly noticed at the edges of the central kerosene/air jet; while at larger radial locations, local equivalence ratio of about 0.02–0.03 is measured in the recirculation zones.

Figure 6 shows radial profiles of local mean equivalence ratio obtained from Fig. 5-b at different axial distances from the exit of the LPP system ($z/D_0$=0.038, 0.38, 0.77, 1.15). As can be seen, the region with little kerosene vapour at the jet periphery is clearly marked on the first three profiles, but vanishes for $z/D_0$=1.15. In addition, little radial expansion of the profiles with axial distance is noted.

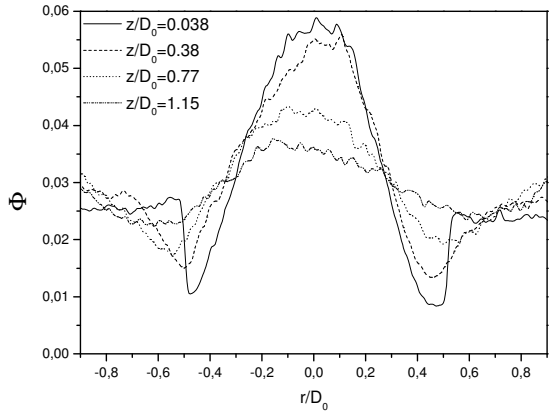


Figure 6. Radial profiles of local mean equivalence ratio at different axial distances for condition 1 (T=500 K, $\Phi_0$=0.12).

**Condition 2 (T=580 K, $\Phi_0$=0.44)**

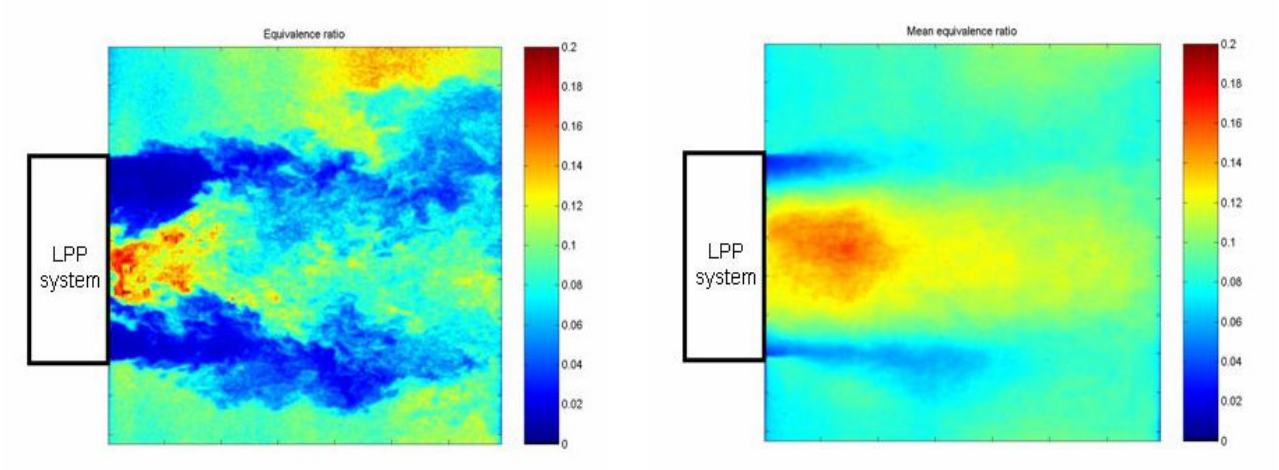


(a) (b)

Figure 7. Instantaneous (a) and average over 200 images (b) maps of local equivalence ratio for condition 2 (T=580 K, $\Phi_0$=0.44).

The second case corresponds to a condition with an inlet temperature of 580 K and an overall equivalence ratio of $\Phi_0$=0.44. Although obtained for a different temperature, comparison with condition 1 helps to characterise the influence of $\Phi_0$ on local equivalence ratio ($\Phi$). An instantaneous map of local equivalence ratio is displayed in Fig. 7-a. Similarly to observations with

condition 1, kerosene vapour is not distributed over all the section of the premixing duct. However, its radial extent at the exit of the LPP system is now $-0.4<r/D_0<0.4$, which is significantly larger than for condition 1. This is due to the larger overall equivalence ratio, hence a larger amount of kerosene fuel injected in the combustor, which enables kerosene vapour to spread at farther radial distance. Nonetheless, a region with a small amount of fuel vapour remains visible at each edge of the duct, although for smaller radial extent than with condition 1. In addition, this region persists axially up to only $z/D_0\sim0.7$ as opposed to $z/D_0\sim1$ for condition 1, Fig. 7-b. The average map of local equivalence ratio in Fig. 7-b indicates that the core of the kerosene/air jet extends over a longer axial distance than with condition 1, due to larger overall equivalence ratio. Figure 7-b also shows that the spatial distribution of $\Phi$ is homogeneous over $z/D_0=0.45$, which is similar to condition 1. However, along the radial dimension, $\Phi$ remains constant around 0.14–0.16 for $-0.2<r/D_0<0.2$, hence slightly larger than for condition 1. In this region, local equivalence ratio lies between 0.14 and 0.16, whereas at larger axial locations, $\Phi$ is about 0.1–0.13. Therefore, the ratio $\Phi/\Phi_0$ is about 35 % at the exit of the LPP system, which is significantly lower than with condition 1. This indicates lower evaporation of kerosene fuel for condition 2, despite higher inlet temperature. Nonetheless, this was expected, because the amount of kerosene to vaporise is about four times larger with condition 2 and the temperature increase is not sufficient to reach similar evaporation rate as with condition 1. It is interesting to notice that the decrease of local equivalence ratio observed for $z/D_0>0.7$ is proportionally less marked than with condition 1, which suggests lower dilution from peripheral air entering the kerosene/air jet. Regions with low equivalence ratio can be observed at the edges of the central kerosene/air jet; although further radially in the recirculation zones, $\Phi$ is about 0.08–0.1, which is larger than with condition 1.

Figure 8 shows radial profiles of local mean equivalence ratio at four axial distances. Similarly to condition 1, the profiles show little radial expansion with axial distance, which indicates that the kerosene/air jet spreads marginally. Regions with low equivalence ratio at the edges of the kerosene/air jet are present on the first three profiles, but vanishes on the last one.

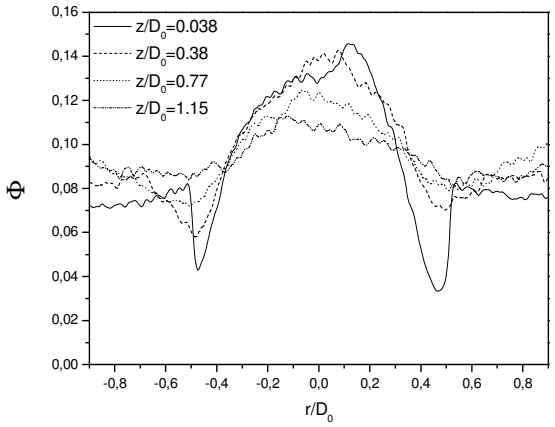


Figure 8. Radial profiles of local mean equivalence ratio at different axial distances for condition 2 (T=580 K, $\Phi_0=0.44$).

## Condition 3 (T=650 K, $\Phi_0=0.44$)

This third case was obtained with an inlet temperature of 650 K and an overall equivalence ratio of $\Phi_0=0.44$. Comparison with condition 2 allows to determine directly the effect of inlet temperature on local equivalence ratio ($\Phi$) because $\Phi_0$ is kept constant between both conditions. An

instantaneous map of local equivalence ratio is presented in Fig. 9-a. Similar observations to condition 2 can be made. The spatial extent of kerosene vapour at the exit of the LPP system extends radially over $-0.4<r/D_0<0.4$. No fuel vapour is detected at each edge of the duct, and this feature also persists axially up to $z/D_0\sim0.7$. In addition, the average map of local equivalence ratio in Fig. 9-b shows that the spatial repartition of $\Phi$ is homogeneous over a region with $-0.2<r/D_0<0.2$ and $0<z/D_0<0.45$. In this region, local equivalence ratio is between 0.2 and 0.24 and decrease to about 0.16 further downstream. This indicates that the ratio $\Phi/\Phi_0$ is of the order of 50 % at the exit of the LPP system, which is larger than with condition 2 ($\Phi/\Phi_0\sim35$ %), but similar to condition 1 ($\Phi/\Phi_0\sim55$ %). This increase of kerosene vaporisation rate between conditions 2 and 3 is due to increase of temperature, which generates more fuel vapour. Comparison between conditions 1 and 3 shows that, in order to observe similar vaporisation rates, it is necessary to increase temperature by 150 K when the amount of kerosene injected is nearly four times more. In the recirculation zones, local equivalence ratio is about 0.1–0.12, hence slightly more than with condition 2, which confirms higher kerosene vaporisation rate here.

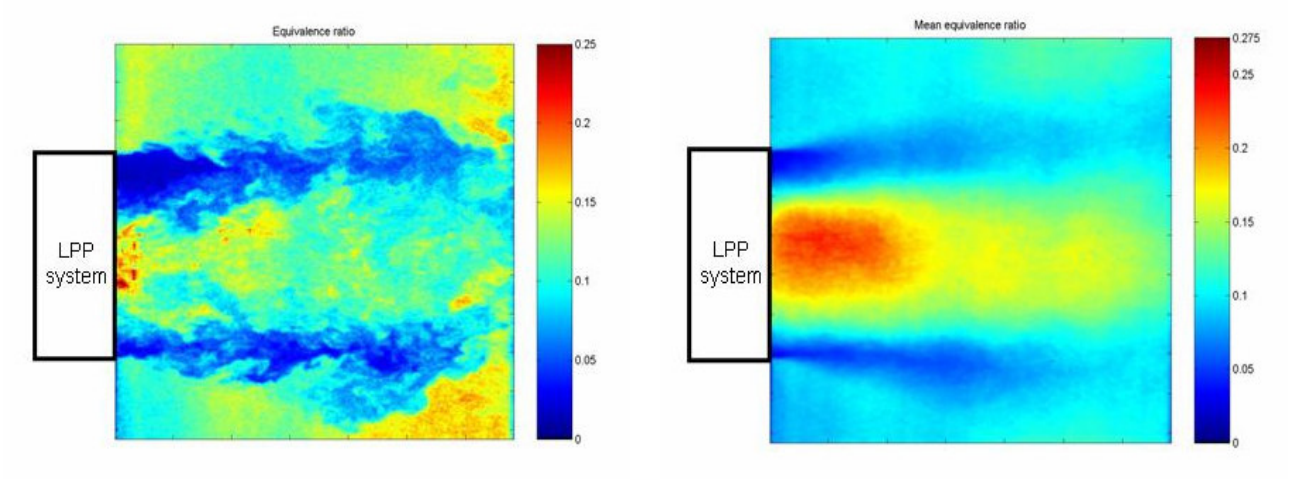


(a) (b)

Figure 9. Instantaneous (a) and average over 200 images (b) maps of local equivalence ratio for condition 3 (T=650 K, $\Phi_0$=0.44).

Figure 10 shows radial profiles of local mean equivalence ratio at different axial distances. Similarly to conditions 1 and 2, the profiles show little radial expansion with axial distance.

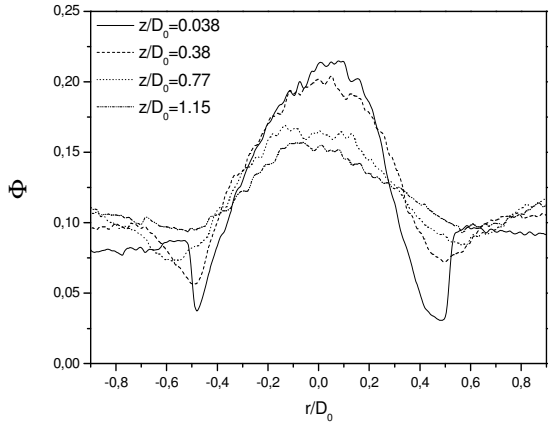


Figure 10. Radial profiles of local mean equivalence ratio at different axial distances for condition 3 (T=650 K, $\Phi_0$=0.44).

## 4. Conclusion

Quantitative PLIF-kerosene was applied for the first time to a LPP injector operating at atmospheric pressure with jet A1 fuel, for air temperature in the range 500–650 K and overall equivalence ratio between 0.12 and 0.44. Single-shot images of kerosene fluorescence were recorded for non-reactive conditions (i.e. no combustion, only fuel vaporisation) with two intensified CCD cameras. Fluorescence images were processed using the dependencies found by Baranger et al. (2005) in order to obtain maps of local equivalence ratio. However, the method was complemented with a new procedure specifically developed for two-phase flows, in order to account for the presence of droplets in the combustor. Influence of inlet temperature and overall equivalence ratio on local equivalence ratio was investigated. Fuel vaporisation rates between 35 and 55 % were obtained, depending on temperature and fuel loading. Downstream from the LPP system, a region of fairly homogeneous equivalence ratio extending axially over half the diameter of the premixing duct was observed. Kerosene fuel did not fully spread over the section of the premixing duct. Instead, there was a region with very little fuel vapour on each side of the duct.

Future experiments are planned to apply the technique to measurements of local equivalence ratio in combusting flows at pressure ranging from 0.1 MPa to 1.0 MPa.

## 5. References

Arnold A., Bombach R., Hubschmid W., Inauen A., Käppeli B. (2000), Fuel-oil concentration in a gas turbine burner measured with laser-induced fluorescence, Exp. in Fluids, Vol. 29, 468-477.

Baranger P., Orain M., Grisch F. (2005), Fluorescence spectroscopy of kerosene vapour: application to gas turbines, AIAA paper N° 2005-828.

Becker J., Hassa C. (2003), Liquid fuel placement and mixing of generic aeroengine premix module at different operating conditions, J. Eng. Gas Turb. Power, Vol. 125, 901-908.

Cheng T.S., Chao Y.C., Wu D.C., Hsu H.W., Yuan T. (2001), Effects of partial premixing on pollutant emissions in swirling methane jet flames, Combustion and Flame, Vol. 125, 865-872.

Cohen J.M., Stufflebeam J.H., Proscia W. (2001), The effect of fuel/air mixing on actuation authority in an active combustion instability control system, J. Eng. Gas Turb. Power, Vol. 123, 537-542.

Correa S.M. (1992), A review of NOx formation under gas-turbine combustion conditions, Combust. Sci. and Tech., Vol. 87, 329-362.

Fric T.F. (1993), Effects of air-fuel unmixedness on NOx emissions, J. of Propulsion and Power, Vol. 9, No.5, 708-713.

Galley D., Pubill Melsio A., Ducruix S., Lacas F., Veynante D. (2004), Experimental study of the dynamics of a LPP injection system, AIAA paper N° 2004-4032.

Greenhalgh D.A. (2000), Laser imaging of fuel injection systems and combustors, Proceeding of the Institution of Mechanical Engineers, Part A: Journal of Power and Energy, Vol. 214, 367-376.

Hicks Y.R., Locke R.J., Anderson R.C., Zaller M., Schock H.J. (1997), Imaging fluorescent combustion species in gas turbine flame tubes: on complexities in real systems, AIAA paper N° 97-2837.

Krämer H., Dinkelacker F., Leipertz A. (1999), Optimization of the mixing quality of real size gas turbine burner with instantaneous planer laser-induced fluorescence imaging, ASME paper N° 99-GT-135.

Lefebvre A.H. (1989), Atomization and sprays, Hemisphere Publishing, 1st Edition.

Lefebvre A.H. (1995), The role of fuel preparation in low emission combustion, J. Eng. Gas Turb. Power, Vol. 117, 617-654.
Lefebvre A.H. (1999), Gas turbines combustion, Taylor & Francis, 2nd Edition.
Lieuwen T., Zinn B.T. (1998), The role of unmixedness in driving combustion instabilities in low NOx gas turbines, 27th Int. Symp. on Comb., 1809-1816.
Locke R.J., Zaller M., Hicks Y.R., Anderson R.C. (1999), Non-intrusive laser-induced imaging for speciation and patternation in high pressure gas turbine combustors, NASA/TM-1999-209395.
Löfström C., Engström J., Richter M., Kaminski C.F., Johansson P., Nyholm K., Hult J., Nygren J., Aldén M. (2000), Feasibility studies and application of laser/optical diagnostics for characterisation of a practical low-emission gas turbine combustor, ASME paper N° 2000-GT-0124.
Löfström C., Kaaling H., Aldén M. (1996), Visualization of fuel distributions in premixed ducts in a low-emission gas turbine combustor using laser techniques, 26th Int. Symp. on Comb., 2787-2793.
Martins G., Cabot G., Taupin B., Vauchelles D., Boukhalfa A. (2004), Experimental study of a lifted LPP flame. LDV, CH chemiluminescence, acetone PLIF measurements, 12th Int. Symp. On Applications of Laser Techniques to Fluid Mechanics, Lisbon, Portugal, 12-15 July 2004, paper 20-5.
Michou Y., Carvahlo I.S., Chauveau C., Gökalp I. (1999), Experimental study of lean premixed and prevaporised turbulent spray combustion, AIAA paper N° 1999-332.
Nguyen Q.V., Mongia, R.K., Dibble R.W. (1999), Real-time optical fuel-to-air ratio sensor for gas turbine combustors, NASA/TM-1999-209041.
Orain M., Mercier X., Grisch F. (2005), PLIF imaging of fuel vapour spatial distribution in an acetone droplet stream, comparison with modelling, Combust. Sci. and Tech., Vol. 177, 249-278.
Pilch M., Erdman C.A. (1987), Use of breakup time data and velocity history data to predict the maximum size of stable fragments for acceleration-induced breakup of a liquid drop, Int. J. Multiphase Flow, Vol. 13, No. 6, 741-757.
Sattelmayer T. (2003), Influence of the combustor aerodynamics on combustion instabilities from equivalence ratio fluctuations, J. Eng. Gas Turb. Power, Vol. 125, 11-19.
Stufflebeam J.H., Kendrick D.W., Sowa W.A., Snyder T.S. (2002), Quantifying fuel/air unmixedness in premixing nozzles using an acetone fluorescence technique, J. Eng. Gas Turb. Power, Vol. 124, 39-45.
Subramaniyam S., Mulemane A., Im K.S., Lai M.C., Tacina R., Tomsik T.M., Lee C.M. (2004), Spray and fuel-air mixing of the swirler/venturi mixers for LPP combustor and fuel reformer applications, AIAA paper N° 2004-0134.
Terasaki T., Hayashi S. (1996), The effects of air-fuel mixing on NOx formation in non-premixed swirl burners, 26th Int. Symp. on Comb., 2733-2739.
Turns S.R. (2000), An introduction to combustion, McGraw-Hill, 2nd Edition.